Central exclusive diffractive production of $p\bar{p}$ pairs in proton-proton collisions at high energies

Piotr Lebiedowicz,[1,*] Otto Nachtmann,[2,†] and Antoni Szczurek[1,‡]

[1]*Institute of Nuclear Physics Polish Academy of Sciences, Radzikowskiego 152, PL-31-342 Kraków, Poland*

[2]*Institut für Theoretische Physik, Universität Heidelberg, Philosophenweg 16, D-69120 Heidelberg, Germany*

(Received 22 January 2018; published 25 May 2018)

We consider the central exclusive production of the $p\bar{p}$ in the continuum and via resonances in proton-proton collisions at high energies. We discuss the diffractive mechanism calculated within the tensor-Pomeron approach including Pomeron, Odderon, and Reggeon exchanges. The theoretical results are discussed in the context of existing WA102 and Intersecting Storage Rings experimental data, and predictions for planned or current experiments at the Relativistic Heavy Ion Collider and the LHC are presented. The distribution in y_{diff}, the rapidity distance between the proton and antiproton, is particularly interesting. We find a dip at $y_{\mathrm{diff}} = 0$ for the $p\bar{p}$ production, in contrast to the $\pi^+\pi^-$ and K^+K^- production. We predict also the $p\bar{p}$ invariant-mass distribution to be less steep than for the pairs of pseudoscalar mesons. We argue that these specific differences for the $p\bar{p}$ production with respect to the pseudoscalar meson pair production can be attributed to the proper treatment of the spin of produced particles. We discuss asymmetries that are due to the interference of $C = +1$ and $C = -1$ amplitudes of $p\bar{p}$ production. We have also calculated the cross section for the $pp \to pp\Lambda\bar{\Lambda}$ reaction. Here, the cross section is smaller, but the characteristic feature for $d\sigma/dy_{\mathrm{diff}}$ is predicted to be similar to $p\bar{p}$ production. The presence of resonances in the $p\bar{p}$ channel may destroy the dip at $y_{\mathrm{diff}} = 0$. This opens the possibility to study diffractively produced resonances. We discuss the observables suited for this purpose.

DOI: 10.1103/PhysRevD.97.094027

I. INTRODUCTION

Diffractive exclusive production of resonances and of dihadron continua are processes with relatively large cross sections, typically of the order of a few μb or even larger. It is expected that central exclusive production, mediated by double Pomeron exchange, is an ideal reaction for the investigation of gluonic bound states (glueballs) of which the existence has not yet been confirmed unambiguously. Observation of glueballs would be a long-awaited confirmation of a crucial prediction of the QCD theory. Such processes were studied extensively at CERN starting from the Intersecting Storage Rings (ISR) experiments [1–5] (for a review, see Ref. [6]) and later at the Omega spectrometer at Super Proton Synchrotron in the fixed-target WA102 experiment; see, e.g., Refs. [7–13]. The measurement of two charged pions in $p\bar{p}$ collisions was performed by the CDF Collaboration at the Tevatron [14]. In this experiment, the outgoing p and $\bar{p}$ were not detected, and only two large rapidity gaps, one on each side of the central hadronic system, were required. Thus, the data include also diffractive dissociation of (anti) protons into undetected hadrons. Exclusive reactions are of particular interest since they can be studied in experiments at the LHC by the ALICE, ATLAS, CMS [15], and LHCb collaborations. At the LHC, in the reactions of interest here, protons are scattered in the forward/backward directions in which relevant detectors are not always present. Recently, there have been several efforts to install and use forward proton detectors. The CMS Collaboration combines efforts with the TOTEM Collaboration, while the ATLAS Collaboration may use the ALFA subdetectors; see, e.g., Ref. [16]. Also, the STAR experiment at the Relativistic Heavy Ion Collider (RHIC) is equipped with such detectors that allow the measurement of forward protons. In this way, the nonexclusive background due to proton breakup could be rejected via the momentum balance constraint [17,18].

*Piotr.Lebiedowicz@ifj.edu.pl
†O.Nachtmann@thphys.uni-heidelberg.de
‡Also at Faculty of Mathematics and Natural Sciences, University of Rzeszów, Pigonia 1, PL-35-310 Rzeszów, Poland. Antoni.Szczurek@ifj.edu.pl

On the theoretical side, the exclusive diffractive dihadron continuum production can be understood as being mainly due to the exchange of two Pomerons between the external protons and the centrally produced hadronic system. First calculations in this respect were concerned with the $pp \to pp\pi^+\pi^-$ reaction [19–21]. The Born amplitude was written in terms of Pomeron/Reggeon exchanges with parameters fixed from phenomenological analyses of NN and πN total and elastic scattering. The four-body amplitude was parametrized using the four-momentum transfers squared t_1, t_2, and s_{ij}, the energies squared in the two-body subsystems. The energy dependence is known from two-body scatterings such as NN, πN, etc. Such calculations make sense for the continuum production of pseudoscalar meson pairs. These model studies were extended also to the $pp \to nn\pi^+\pi^+$ [22] and $pp \to ppK^+K^-$ [23] reactions and even for the exclusive $\pi^+\pi^-\pi^+\pi^-$ continuum production [24]. In reality, the Born approximation is usually not sufficient, and absorption corrections have to be taken into account; see, e.g., Refs. [25,26]. The phenomenological concepts underlying these calculations require further tests and clear phenomenological evidence to be commonly accepted.

In this paper, we are concerned with reactions in which the exchange of the soft Pomeron plays the most important role. This—still somewhat enigmatic—soft Pomeron is a flavorless object. It is often loosely stated that it possesses quantum numbers of the vacuum. This is true for the internal quantum numbers of the Pomeron. However, the spin structure of the soft Pomeron certainly is not that of the vacuum, i.e., spin 0. We believe that the soft Pomeron is best described as an effective rank-2 symmetric-tensor exchange as introduced in Ref. [27]. In Ref. [28], three hypotheses for the soft-Pomeron spin structure, effective scalar, vector, and tensor exchange were discussed and compared to the experimental data on the helicity structure of proton-proton elastic scattering at $\sqrt{s} = 200$ GeV and small $|t|$ from the STAR experiment [29]. Only the tensor option was shown to be viable; the vector and scalar options for the soft Pomeron could be excluded. In Ref. [28], also some remarks on the history of the views of the Pomeron spin structure were presented. For the convenience of the reader, we repeat here some of the main points concerning the tensor Pomeron in its connection to QCD. In Ref. [30], one of us made a general investigation of high-energy soft diffractive processes in QCD using functional methods. It was shown there that the resulting soft Pomeron could be described as coherent exchange of spin $2 + 4 + 6 + \cdots$. This is exactly the structure of the tensor Pomeron of Ref. [27]; see Appendix B there. In this way, the tensor Pomeron of Ref. [27] has good backing in nonperturbative QCD. Also, investigations in the framework of the AdS/CFT correspondence prefer a tensor nature for the soft-Pomeron exchange [31,32].

First applications of the tensor-Pomeron model of Ref. [27] to the central exclusive production (CEP) of several scalar and pseudoscalar mesons in the reaction $pp \to ppM$ were studied in Ref. [33] for the relatively low WA102 energy, in which also the secondary Reggeon exchanges play a very important role. The resonant ρ^0 ($J^{PC} = 1^{--}$) and nonresonant (Drell-Söding) $\pi^+\pi^-$ photoproduction contributions to CEP were studied in Ref. [34]. In Ref. [35], an extensive study of the reaction $\gamma p \to \pi^+\pi^- p$ was presented. In Ref. [36], the model was applied to the reaction $pp \to pp\pi^+\pi^-$ including the dipion continuum, the dominant scalar $f_0(500)$, $f_0(980)$ ($J^{PC} = 0^{++}$), and tensor $f_2(1270)$ ($J^{PC} = 2^{++}$) resonances decaying into the $\pi^+\pi^-$ pairs. In Ref. [37], the model was applied to the $\pi^+\pi^-\pi^+\pi^-$ production via the intermediate $\sigma\sigma$ and $\rho^0\rho^0$ states. Also, the ρ^0 meson production associated with a very forward/backward πN system, that is, the $pp \to pp\rho^0\pi^0$ and $pp \to pn\rho^0\pi^+$ processes, were discussed in Ref. [38]. It was shown in Refs. [33–38] that the tensor-Pomeron model does quite well in reproducing the data where available.

Closely related to the reaction $pp \to ppp\bar{p}$ studied by us here are the reactions of central $p\bar{p}$ production in ultraperipheral nucleus-nucleus and nucleon-nucleus collisions, $AA \to AAp\bar{p}$ and $pA \to pAp\bar{p}$. For the first process, see Ref. [39], in which the parameters of the model including the proton exchange, the $f_2(1270)$ and $f_2(1950)$ s-channel exchanges, and the handbag mechanism were fitted to Belle data [40] for the $\gamma\gamma \to p\bar{p}$ reaction. The model was applied then to estimate the cross section for the ultraperipheral, ultrarelativistic, heavy-ion collisions at the LHC.

In the following, we extend the application of the tensor-Pomeron model to central exclusive production of spin-1/2 hadron pairs ($p\bar{p}$ or $\Lambda\bar{\Lambda}$) in pp collisions. The centrally produced baryon-antibaryon pairs were studied experimentally in Refs. [2,4,10]. So far, the $pp \to ppp\bar{p}$ reaction at LHC energies has not been considered from the theory point of view. We will show first predictions for this reaction in the tensor-Pomeron approach and compare them with results for central production of dihadrons with spin 0, $\pi^+\pi^-$, and K^+K^-. We shall discuss whether the predictions of the tensor-Pomeron model can be verified by planned measurements at the RHIC and at the LHC. The observables suited for this purpose shall be presented.

Our paper is organized as follows. In Sec. II, we discuss continuum $p\bar{p}$ production. Section III deals with $p\bar{p}$ production via scalar resonances. First results are presented in Secs. IV and V presents our conclusions. We include in our calculations the exchanges of the soft Pomeron, of Reggeons, and also of the soft Odderon for some distributions. The Odderon was introduced a long time ago [41,42] (for a review, see, e.g., Ref. [43]) and has recently become very interesting again [44–47].

We want to emphasize that the purpose of our paper is not to compare predictions of our tensor-Pomeron approach with alternatives for the soft-Pomeron structure. This has been done extensively in Refs. [28,33]. Also, since we are interested in the soft-scattering regime, we

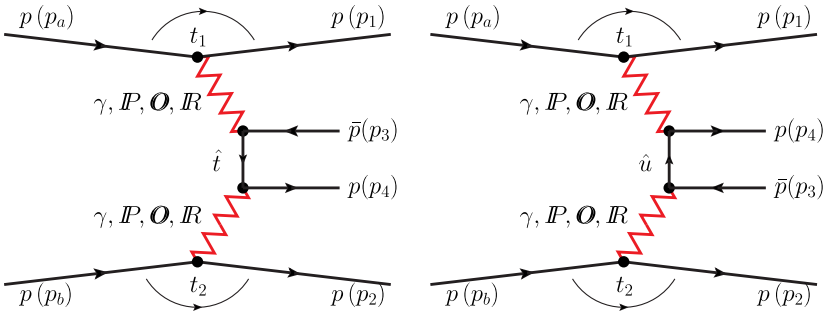

FIG. 1. The Born diagrams for the double Pomeron/Reggeon and photon-mediated central exclusive continuum $p\bar{p}$ production in proton-proton collisions.

cannot use or compare with the perturbative Pomeron, initiated in Refs. [48–51]. The purpose of our work is to give experimentalists a solid idea of what to expect theoretically in central exclusive $p\bar{p}$ production. What are the magnitudes of cross sections? Where is continuum $p\bar{p}$? Where is resonance production prominent? What is the role of secondary Reggeon exchanges and, if it exists, of Odderon exchange? What are the differences between $p\bar{p}$ and two pseudoscalars central production? We would hope that our calculations could serve as basis for the construction of an event generator for this and related processes.[1] A long-term goal would be to derive the coupling constants of our effective theory from nonperturbative QCD, but this is beyond the scope of the present paper.

II. $p\bar{p}$ CONTINUUM PRODUCTION

We study central exclusive production of $p\bar{p}$ in proton-proton collisions at high energies

$$p(p_a,\lambda_a)+p(p_b,\lambda_b) \to p(p_1,\lambda_1)+\bar{p}(p_3,\lambda_3)+p(p_4,\lambda_4)+p(p_2,\lambda_2), \tag{2.1}$$

where p_i and $\lambda_i \in \{+1/2,-1/2\}$, indicated in brackets, denote the 4-momenta and helicities of the nucleons, respectively. The $\mathcal{T}$-matrix element for the reaction (2.1) will be denoted as follows:

$$\mathcal{M}_{\lambda_a\lambda_b\to\lambda_1\lambda_2\lambda_3\lambda_4} = \langle p(p_1,\lambda_1), p(p_4,\lambda_4), \bar{p}(p_3,\lambda_3)p(p_2,\lambda_2) |\mathcal{T}|p(p_a,\lambda_a), p(p_b,\lambda_b)\rangle. \tag{2.2}$$

Note that the order of the particles in the bra and ket states matters since we are dealing with fermions.

In general, the full amplitude for the $p\bar{p}$ production is a sum of the continuum amplitude and the amplitudes with the s-channel resonances:

$$\mathcal{M}_{\lambda_a\lambda_b\to\lambda_1\lambda_2\lambda_3\lambda_4} = \mathcal{M}^{p\bar{p}\text{-continuum}}_{\lambda_a\lambda_b\to\lambda_1\lambda_2\lambda_3\lambda_4} + \mathcal{M}^{p\bar{p}\text{-resonances}}_{\lambda_a\lambda_b\to\lambda_1\lambda_2\lambda_3\lambda_4}. \tag{2.3}$$

At high energies, the exchange objects to be considered are the photon γ, the Pomeron $\mathbb{P}$, the Odderon $\mathbb{O}$, and the Reggeons $\mathbb{R}$. Their charge-conjugation and G-parity quantum numbers are listed in Table I of Ref. [36]. We treat the $C=+1$ Pomeron and the Reggeons $\mathbb{R}_+ = f_{2\mathbb{R}}, a_{2\mathbb{R}}$ as effective tensor exchanges, while the $C=-1$ Odderon and the Reggeons $\mathbb{R}_- = \omega_{\mathbb{R}}, \rho_{\mathbb{R}}$ are treated as effective vector exchanges.

The $p\bar{p}$ continuum amplitude is expressed as the sum of $\hat{t}$ and $\hat{u}$ diagrams shown in Fig. 1,

$$\mathcal{M}^{p\bar{p}-\text{continuum}}_{\lambda_a\lambda_b\to\lambda_1\lambda_2\lambda_3\lambda_4} = \mathcal{M}^{(\hat{t})}_{\lambda_a\lambda_b\to\lambda_1\lambda_2\lambda_3\lambda_4} + \mathcal{M}^{(\hat{u})}_{\lambda_a\lambda_b\to\lambda_1\lambda_2\lambda_3\lambda_4}. \tag{2.4}$$

The combinations (C_1, C_2) of exchanges that can contribute in (2.4) are

$$(C_1,C_2)=(1,1)\colon\ (\mathbb{P}+\mathbb{R}_+, \mathbb{P}+\mathbb{R}_+); \tag{2.5}$$

$$(C_1,C_2)=(-1,-1)\colon\ (\mathbb{O}+\mathbb{R}_-+\gamma, \mathbb{O}+\mathbb{R}_-+\gamma); \tag{2.6}$$

$$(C_1,C_2)=(1,-1)\colon\ (\mathbb{P}+\mathbb{R}_+, \mathbb{O}+\mathbb{R}_-+\gamma); \tag{2.7}$$

$$(C_1,C_2)=(-1,1)\colon\ (\mathbb{O}+\mathbb{R}_-+\gamma, \mathbb{P}+\mathbb{R}_+). \tag{2.8}$$

Here, C_1 and C_2 are the charge-conjugation quantum numbers of the exchange objects. The contributions involving the photon γ in Eqs. (2.6)–(2.8) are expected to be small but may be important at very small four-momentum transfer squared. The $(\gamma, \mathbb{P}+\mathbb{R}_+)$ and $(\mathbb{P}+\mathbb{R}_+, \gamma)$ contributions will be very important for the $p\bar{p}$ production in pA collisions. There, one also has to take into account contact terms required by gauge invariance. This will be studied elsewhere. The contributions involving the Odderon $\mathbb{O}$ are expected to be small since its coupling to the proton is very small. Thus, we shall concentrate on the diffractive production of $p\bar{p}$ through the $\mathbb{P}$, $\mathbb{R}_+$, and $\mathbb{R}_-$ exchanges but also mention Odderon effects where appropriate.

[1]The GenEx Monte Carlo generator [52] could be used and expanded in this context.

The kinematic variables for reaction (2.1) are

$$s=(p_a+p_b)^2=(p_1+p_2+p_3+p_4)^2,\qquad s_{ij}=(p_i+p_j)^2,\qquad s_{34}=M_{34}^2=(p_3+p_4)^2,\qquad t_1=q_1^2,$$
$$q_1=p_a-p_1,\qquad t_2=q_2^2,\qquad q_2=p_b-p_2,\qquad \hat{p}_t=p_a-p_1-p_3,\qquad \hat{p}_u=p_4-p_a+p_1. \tag{2.9}$$

Let us first take a look at the dominant ($\mathbb{P}$, $\mathbb{P}$) contribution. The t̂- and û-channel amplitudes for the $\mathbb{P}\mathbb{P}$ exchange can be written as

$$\begin{aligned}\mathcal{M}^{(\hat{t})}_{\lambda_a\lambda_b\to\lambda_1\lambda_2\lambda_3\lambda_4}&=(-i)\bar{u}(p_1,\lambda_1)i\Gamma^{(\mathbb{P}pp)}_{\mu_1\nu_1}(p_1,p_a)u(p_a,\lambda_a)i\Delta^{(\mathbb{P})\mu_1\nu_1,\alpha_1\beta_1}(s_{13},t_1)\\&\times\bar{u}(p_4,\lambda_4)i\Gamma^{(\mathbb{P}pp)}_{\alpha_2\beta_2}(p_4,\hat{p}_t)iS_F(\hat{p}_t)i\Gamma^{(\mathbb{P}pp)}_{\alpha_1\beta_1}(\hat{p}_t,-p_3)v(p_3,\lambda_3)\\&\times i\Delta^{(\mathbb{P})\alpha_2\beta_2,\mu_2\nu_2}(s_{24},t_2)\bar{u}(p_2,\lambda_2)i\Gamma^{(\mathbb{P}pp)}_{\mu_2\nu_2}(p_2,p_b)u(p_b,\lambda_b),\end{aligned} \tag{2.10}$$

$$\begin{aligned}\mathcal{M}^{(\hat{u})}_{\lambda_a\lambda_b\to\lambda_1\lambda_2\lambda_3\lambda_4}&=(-i)\bar{u}(p_1,\lambda_1)i\Gamma^{(\mathbb{P}pp)}_{\mu_1\nu_1}(p_1,p_a)u(p_a,\lambda_a)i\Delta^{(\mathbb{P})\mu_1\nu_1,\alpha_1\beta_1}(s_{14},t_1)\\&\times\bar{u}(p_4,\lambda_4)i\Gamma^{(\mathbb{P}pp)}_{\alpha_1\beta_1}(p_4,\hat{p}_u)iS_F(\hat{p}_u)i\Gamma^{(\mathbb{P}pp)}_{\alpha_2\beta_2}(\hat{p}_u,-p_3)v(p_3,\lambda_3)\\&\times i\Delta^{(\mathbb{P})\alpha_2\beta_2,\mu_2\nu_2}(s_{23},t_2)\bar{u}(p_2,\lambda_2)i\Gamma^{(\mathbb{P}pp)}_{\mu_2\nu_2}(p_2,p_b)u(p_b,\lambda_b).\end{aligned} \tag{2.11}$$

Here, we use the standard propagator for the proton $iS_F(\hat{p})=i/(\hat{\not{p}}-m_p)$. The effective propagator of the tensor-Pomeron exchange and the Pomeron-proton vertex function are given in Sec. 3 of Ref. [27]. For the convenience of the reader, we collect these and other quantities, which we use in our work in Appendix.

For $\mathbb{P}\mathbb{P}$ fusion, the centrally produced $p\bar{p}$ system is in a state of $C=+1$. This implies for the amplitude (2.2) the following:

$$\begin{aligned}&\langle p(p_1,\lambda_1),p(p_4,\lambda_4),\bar{p}(p_3,\lambda_3),p(p_2,\lambda_2)|\mathcal{T}|p(p_a,\lambda_a),p(p_b,\lambda_b)\rangle^{(\mathbb{P},\mathbb{P})}\\&=\langle p(p_1,\lambda_1),\bar{p}(p_4,\lambda_4),p(p_3,\lambda_3),p(p_2,\lambda_2)|\mathcal{T}|p(p_a,\lambda_a),p(p_b,\lambda_b)\rangle^{(\mathbb{P},\mathbb{P})}\\&=-\langle p(p_1,\lambda_1),p(p_3,\lambda_3),\bar{p}(p_4,\lambda_4),p(p_2,\lambda_2)|\mathcal{T}|p(p_a,\lambda_a),p(p_b,\lambda_b)\rangle^{(\mathbb{P},\mathbb{P})}.\end{aligned} \tag{2.12}$$

Here, we work in the overall c.m. system and assume that the helicity states for the centrally produced p and $\bar{p}$ are both taken of the same type, e.g., of type a; see Appendix of Ref. [39]. This antisymmetry relation (2.12) can, of course, be verified explicitly using the expressions for $\mathcal{M}^{(\hat{t})}$ and $\mathcal{M}^{(\hat{u})}$ from Eqs. (2.10) and (2.11), respectively.

If we use another choice of p and $\bar{p}$ helicity states in the c.m. system, we will get additional phase factors in (2.12) and the corresponding relations for the other (C_1,C_2) exchanges. But these phase factors drop out for distributions in which the polarizations of the centrally produced p and $\bar{p}$ are not observed. Thus, our above choice for the p and $\bar{p}$ helicity states is very convenient as it makes the $p\bar{p}$ charge-conjugation relations for the amplitudes simple and explicit.

The antisymmetry relation (2.12) holds for all exchanges with $(C_1,C_2)=(1,1)$ and $(-1,-1)$; see Eqs. (2.5) and (2.6). For the exchanges with $(C_1,C_2)=(1,-1)$ and $(-1,1)$, we have, instead, symmetry under the exchange $(p(p_4,\lambda_4),\bar{p}(p_3,\lambda_3))\to(p(p_3,\lambda_3),\bar{p}(p_4,\lambda_4))$; see Eqs. (2.7) and (2.8).

In the high-energy approximation, we can write the $\mathbb{P}\mathbb{P}$-exchange amplitude as

$$\begin{aligned}\mathcal{M}^{(\mathbb{P}\mathbb{P}\to p\bar{p})}_{\lambda_a\lambda_b\to\lambda_1\lambda_2\lambda_3\lambda_4}&\simeq(3\beta_{\mathbb{P}NN})^2 2(p_1+p_a)_{\mu_1}(p_1+p_a)_{\nu_1}\delta_{\lambda_1\lambda_a}[F_1(t_1)]^2\\&\times\bar{u}(p_4,\lambda_4)\Big[\gamma^{\mu_2}(p_4+\hat{p}_t)^{\nu_2}\frac{1}{4s_{13}}(-is_{13}\alpha'_{\mathbb{P}})^{\alpha_{\mathbb{P}}(t_1)-1}\frac{[\hat{F}_p(\hat{p}_t^2)]^2}{\hat{\not{p}}_t-m_p}\gamma^{\mu_1}(\hat{p}_t-p_3)^{\nu_1}\frac{1}{4s_{24}}(-is_{24}\alpha'_{\mathbb{P}})^{\alpha_{\mathbb{P}}(t_2)-1}\\&+\gamma^{\mu_1}(p_4+\hat{p}_u)^{\nu_1}\frac{1}{4s_{14}}(-is_{14}\alpha'_{\mathbb{P}})^{\alpha_{\mathbb{P}}(t_1)-1}\frac{[\hat{F}_p(\hat{p}_u^2)]^2}{\hat{\not{p}}_u-m_p}\gamma^{\mu_2}(\hat{p}_u-p_3)^{\nu_2}\frac{1}{4s_{23}}(-is_{23}\alpha'_{\mathbb{P}})^{\alpha_{\mathbb{P}}(t_2)-1}\Big]v(p_3,\lambda_3)\\&\times(3\beta_{\mathbb{P}NN})^2 2(p_2+p_b)_{\mu_2}(p_2+p_b)_{\nu_2}\delta_{\lambda_2\lambda_b}[F_1(t_2)]^2.\end{aligned} \tag{2.13}$$

In Eq. (2.13), we have introduced a form factor $\hat{F}_p(\hat{p}^2)$, taking into account that the intermediate protons in Fig. 1 are off shell. This proton off-shell form factor is parametrized here in the exponential form,

$$\hat{F}_p(\hat{p}^2) = \exp\left(\frac{\hat{p}^2 - m_p^2}{\Lambda^2_{\text{off},E}}\right), \tag{2.14}$$

where $\Lambda_{\text{off},E}$ has to be adjusted to experimental data. The form factor (2.14) is normalized to unity at the on-shell point $\hat{p}^2 = m_p^2$.

In a way similar to Eqs. (2.10)–(2.13), we can write the amplitudes for the exchanges $(\mathbb{P}, \mathbb{R}_+)$, $(\mathbb{R}_+, \mathbb{P})$, and $(\mathbb{R}_+, \mathbb{R}_+)$, since both $\mathbb{P}$ and $\mathbb{R}_+$ exchange are treated as tensor exchanges in our model. The contributions in Eqs. (2.6)–(2.8) involving $C = -1$ exchanges are different. We recall that $\mathbb{R}_-$ exchanges are treated as effective vector exchanges in our model; see Sec. 3 of Ref. [27] and Appendix of the present paper.

III. $pp \to pp(f_0 \to p\bar{p})$

The resonances produced diffractively in the $p\bar{p}$ channel are not well known. Therefore, we will concentrate only on the s-channel scalar resonances. We shall study the reaction $pp \to pp(f_0 \to p\bar{p})$, where f_0 stands for one of the $f_0(2020)$, $f_0(2100)$, and $f_0(2200)$ states with $I^G(J^{PC}) = 0^+(0^{++})$. It must be noted that these states are only listed in Ref. [53] and are not included in the summary tables. Also, their couplings to the $p\bar{p}$ channel are essentially unknown.

The $\mathbb{PP}$-exchange amplitude through a scalar resonance $f_0 \to p\bar{p}$ can be written as

$$\begin{aligned}\mathcal{M}^{(\mathbb{PP}\to f_0\to p\bar{p})}_{\lambda_a\lambda_b\to\lambda_1\lambda_2\lambda_3\lambda_4} \simeq\ & 3\beta_{\mathbb{P}NN} 2(p_1+p_a)_{\mu_1}(p_1+p_a)_{\nu_1}\delta_{\lambda_1\lambda_a}F_1(t_1)\frac{1}{4s_1}(-is_1\alpha'_{\mathbb{P}})^{\alpha_{\mathbb{P}}(t_1)-1} \\ & \times \Gamma^{(\mathbb{PP}f_0)\mu_1\nu_1,\mu_2\nu_2}(q_1,q_2)\Delta^{(f_0)}(p_{34})\bar{u}(p_4,\lambda_4)\Gamma^{(f_0p\bar{p})}(p_4,-p_3)v(p_3,\lambda_3) \\ & \times \frac{1}{4s_2}(-is_2\alpha'_{\mathbb{P}})^{\alpha_{\mathbb{P}}(t_2)-1} 3\beta_{\mathbb{P}NN} 2(p_2+p_b)_{\mu_2}(p_2+p_b)_{\nu_2}\delta_{\lambda_2\lambda_b}F_1(t_2),\end{aligned} \tag{3.1}$$

where $s_1 = (p_1 + p_3 + p_4)^2$, $s_2 = (p_2 + p_3 + p_4)^2$, and $p_{34} = p_3 + p_4$.

The effective Lagrangians and the vertices for $\mathbb{PP}$ fusion into an f_0 meson are discussed in Appendix of Ref. [33]. As was shown there, the tensorial $\mathbb{PP}f_0$ vertex corresponds to the sum of the two lowest values of (l, S), that is, $(l, S) = (0, 0)$ and (2,2) with coupling parameters $g'_{\mathbb{PP}f_0}$ and $g''_{\mathbb{PP}f_0}$, respectively. The vertex, including a form factor, reads then as follows ($p_{34} = q_1 + q_2$):

$$\begin{aligned}i\Gamma^{(\mathbb{PP}f_0)}_{\mu\nu,\kappa\lambda}(q_1,q_2) =\ & \left(i\Gamma'^{(\mathbb{PP}f_0)}_{\mu\nu,\kappa\lambda}\Big|_{\text{bare}} + i\Gamma''^{(\mathbb{PP}f_0)}_{\mu\nu,\kappa\lambda}(q_1,q_2)\Big|_{\text{bare}}\right) \\ & \times \tilde{F}^{(\mathbb{PP}f_0)}(q_1^2,q_2^2,p_{34}^2);\end{aligned} \tag{3.2}$$

see Eq. (A.21) of Ref. [33]. As was shown in Ref. [33], these two (l, S) couplings give different results for the distribution in the azimuthal angle between the transverse momenta $\vec{p}_{t,1}$ and $\vec{p}_{t,2}$ of the outgoing leading protons. We take the factorized form for the Pomeron-Pomeron-meson form factor

$$\tilde{F}^{(\mathbb{PP}f_0)}(q_1^2,q_2^2,p_{34}^2) = F_M(q_1^2)F_M(q_2^2)F^{(\mathbb{PP}f_0)}(p_{34}^2) \tag{3.3}$$

normalized to $\tilde{F}^{(\mathbb{PP}f_0)}(0,0,m_{f_0}^2) = 1$. We will further set

$$F^{(\mathbb{PP}f_0)}(p_{34}^2) = \exp\left(\frac{-(p_{34}^2 - m_{f_0}^2)^2}{\Lambda_{f_0}^4}\right),$$
$$\Lambda_{f_0} = 1 \text{ GeV}. \tag{3.4}$$

The scalar-meson propagator is taken as

$$i\Delta^{(f_0)}(p_{34}) = \frac{i}{p_{34}^2 - m_{f_0}^2 + im_{f_0}\Gamma_{f_0}}, \tag{3.5}$$

with constant widths for the f_0 states with the numerical values from Ref. [53].

For the $f_0 p\bar{p}$ vertex, we have

$$i\Gamma^{(f_0p\bar{p})}(p_4,-p_3) = ig_{f_0p\bar{p}}F^{(f_0p\bar{p})}(p_{34}^2), \tag{3.6}$$

where $g_{f_0p\bar{p}}$ is an unknown dimensionless parameter. We assume $g_{f_0p\bar{p}} > 0$ and $F^{(f_0p\bar{p})}(p_{34}^2) = F^{(\mathbb{PP}f_0)}(p_{34}^2)$; see Eq. (3.4).

IV. FIRST RESULTS

We start our analysis by comparing the cross section of our nonresonant contribution to the $pp \to ppp\bar{p}$ reaction (2.1) with the CERN ISR data at $\sqrt{s} = 62$ GeV [4]. In Ref. [4], the centrally produced antiproton and proton were restricted to lie in the rapidity regions $|y_3|$, $|y_4| < 1.5$, respectively, and the outgoing forward protons to have $x_{F,p} > 0.9$ and the four-momentum transfer squared $|t| \geq 0.08$ GeV^2. With such kinematic conditions, we get the integrated cross section of $\sigma_{\text{th}} = 0.013$ and 0.236 μb for $\Lambda_{\text{off},E} = 0.8$ and 1 GeV, respectively, compared with $\sigma_{\text{exp}} = 0.80 \pm 0.17$ μb from Ref. [4]. Our theoretical results have been obtained in the Born approximation (neglecting absorptive corrections). The realistic cross section can be obtained by multiplying the Born cross section by the corresponding gap survival factor $\langle S^2 \rangle$. At the ISR energies, we estimate it to be $\langle S^2 \rangle \simeq 0.5$.[2] In our

[2]In exclusive reactions, as the $pp \to pp\pi^+\pi^-$ one, for instance, the gap survival factor is strongly dependent on the t_1 and t_2 variables; see, e.g., Refs. [26,34].

TABLE I. The integrated cross sections in μb for the exclusive diffractive $p\bar{p}$ continuum production for some experimental cuts on (pseudo)rapidity and p_t of centrally produced individual p and $\bar{p}$ for the STAR, ALICE, ATLAS, CMS, and LHCb experiments. Results for some limitations on leading protons are also shown. The column "$\mathbb{P}$ and $\mathbb{R}$" shows the resulting total cross sections from $\mathbb{P}$ and $\mathbb{R}$ ($\mathbb{R}_+$ and $\mathbb{R}_-$) exchanges, which include, of course, the interference term between the various components. The column "$\mathbb{P}$" shows results obtained for the $\mathbb{P}$ exchange alone. We have taken here $\Lambda_{\text{off},E} = 1$ GeV. No absorption effects were included here.

$\sqrt{s}$, TeV	Cuts	$\mathbb{P}$ and $\mathbb{R}$	$\mathbb{P}$
0.2	$\lvert\eta\rvert < 1$, $p_t > 0.2$ GeV	0.031	0.018
0.2	$\lvert\eta\rvert < 1$, $p_t > 0.2$ GeV, $0.03 < -t_{1,2} < 0.3$ GeV^2	0.014	0.008
13	$\lvert\eta\rvert < 0.9$, $p_t > 0.1$ GeV	0.032	0.031
13	$\lvert y\rvert < 2$, $p_t > 0.2$ GeV	2.38	2.19
13	$\lvert\eta\rvert < 2.5$, $p_t > 0.1$ GeV	1.96	1.82
13	$\lvert\eta\rvert < 2.5$, $p_t > 0.1$ GeV, $0.17 < \lvert p_y\rvert < 0.5$ GeV	0.31	0.29
13	$2 < \eta < 4.5$, $p_t > 0.2$ GeV	0.79	0.68

calculations, we include the Pomeron and Reggeon $\mathbb{R}_+$ and $\mathbb{R}_-$ exchanges; see Eqs. (2.5)–(2.8). For double-Pomeron exchange and $\Lambda_{\text{off},E} = 1$ GeV, we get only $\sigma_{\text{th}} = 0.077$ μb. It is seen that inclusion of subleading Reggeon exchanges is crucial at the ISR energy. In Ref. [2], the measurement was performed at $\sqrt{s} = 63$ GeV, $|y_3|, |y_4| \le 1$, $x_{F,p} > 0.95$, $0.01 \lesssim |t| \lesssim 0.06$ GeV^2, and the cross section $d^2\sigma_{\text{exp}}/dt_1 dt_2 = 1.0 \pm 0.5$ μb GeV^{-4} for $t_1 = t_2 = -0.035$ GeV^2 was determined. We get (without absorption) $d^2\sigma_{\text{th}}/dt_1 dt_2 = 0.73$ and 14.14 μb GeV^{-4} for $\Lambda_{\text{off},E} = 0.8$ and 1 GeV, respectively. We see that this experiment supports the smaller value of $\Lambda_{\text{off},E}$. Although the ISR experiments [2,4] were performed for different kinematic coverage in both, an enhancement in the low $p\bar{p}$ invariant-mass region was observed. The low-mass enhancement is clearly seen also at the WA102 energy [10]; see Fig. 1(b) there. Therefore, the nonresonant (continuum) contribution alone is not sufficient to describe the low-energy data, and, e.g., scalar and/or tensor resonance contributions should be taken into account. We will return to this issue below (see Fig. 9).

Now, we show numerical results for the reaction $pp \to ppp\bar{p}$ at higher energies. In Table I, we have collected cross sections in μb for the exclusive $p\bar{p}$ continuum including some experimental cuts. We show results for the Pomeron and Reggeon exchanges in the amplitude (see the column "$\mathbb{P}$ and $\mathbb{R}$") and when only the $(\mathbb{P},\mathbb{P})$ term contributes (see the column "$\mathbb{P}$"). The calculations have been done in the Born approximation (without absorption effects) and for $\Lambda_{\text{off},E} = 1$ GeV in Eq. (2.14). The absorption effects lead to a damping of the cross section by a factor 5 for $\sqrt{s} = 0.2$ TeV and by a factor 10 for $\sqrt{s} = 13$ TeV; see, e.g. Ref. [26]. The next-to-last line in Table I shows result with an extra cut on leading protons of 0.17 GeV $< |p_{y,1}|, |p_{y,2}| < 0.5$ GeV that will be measured in ALFA on both sides of the ATLAS detector.

We have also calculated the corresponding cross sections for the $pp \to pp\Lambda\bar{\Lambda}$ reaction, taking into account only the dominant $(\mathbb{P},\mathbb{P})$ contribution. The amplitude $\mathcal{M}^{(\mathbb{P}\mathbb{P}\to\Lambda\bar{\Lambda})}$ is very much the same as $\mathcal{M}^{(\mathbb{P}\mathbb{P}\to p\bar{p})}$ (2.13) but with m_p, $\hat{F}_p$ replaced by m_Λ, $\hat{F}_\Lambda$. To describe the off-shellness of the intermediate t/u-channel Λ baryons, we assume the form factor given by Eq. (2.14) with $\Lambda_{\text{off},E} = 1$ GeV. For the coupling of the Λ baryon to the Pomeron, we make an ansatz similar to the proton-Pomeron coupling in Eq. (A4) of Appendix but with $\beta_{\mathbb{P}NN}$ replaced by a constant $\beta_{\mathbb{P}\Lambda\Lambda}$. The value of the latter can be estimated from the data on the total cross sections for Λp and pp scattering at high energies[3] using Eq. (6.41) of Ref. [27]:

$$\beta_{\mathbb{P}\Lambda\Lambda} \cong \beta_{\mathbb{P}NN}\frac{\sigma_{\text{tot}}(\Lambda p)}{\sigma_{\text{tot}}(pp)} \cong 1.87\ \text{GeV}^{-1} \times 0.9 \simeq 1.68\ \text{GeV}^{-1}. \tag{4.1}$$

We find a cross section of 0.11 μb for $\sqrt{s} = 13$ TeV and the ATLAS cuts ($|\eta| < 2.5$, $p_t > 0.1$ GeV on centrally produced Λ and $\bar{\Lambda}$ baryons) and a cross section of 0.04 μb for the LHCb cuts ($2 < \eta < 4.5$ and $p_t > 0.2$ GeV). The calculated cross section for the $\Lambda\bar{\Lambda}$ continuum production is about 16 times smaller than the corresponding $p\bar{p}$ continuum production one.

In Figs. 2 and 3, we present the distributions in the $p\bar{p}$ invariant mass M_{34}, in the antiproton rapidity y_3, and in the rapidity distance between the antiproton and proton $y_{\text{diff}} = y_3 - y_4$ at $\sqrt{s} = 13$ TeV. We wanted to concentrate only on the main characteristics of the $p\bar{p}$ continuum production; therefore, the calculations have been done neglecting the absorptive corrections. To illustrate uncertainties of our model, we take in the calculation two values of $\Lambda_{\text{off},E}$; see Eq. (2.14). The black long-dashed line represents the result for $\Lambda_{\text{off},E} = 1$ GeV, and the black short-dashed line represents the result for $\Lambda_{\text{off},E} = 0.8$ GeV. For comparison, we also show results for the $\pi^+\pi^-$ and K^+K^- continuum production; see the blue solid line and the blue dotted line, respectively. The reaction $pp \to pp\pi^+\pi^-$ was discussed already in Ref. [36]. The reaction $pp \to ppK^+K^-$ in the

[3]The Λp total cross sections were measured in Refs. [54–57]. In Ref. [57], the average cross section was obtained as $\sigma_{\text{tot}}(\Lambda p) = 34.6 \pm 0.4$ mb in the hyperon momentum interval $P_{\text{lab}} =$ 6–21 GeV (which corresponds to $\sqrt{s} \sim 4$–6 GeV). The lack of $\sigma_{\text{tot}}(\Lambda p)$ data at higher energy does not allow any reasonable estimate of the ratio, $\sigma_{\text{tot}}(\Lambda p)/\sigma_{\text{tot}}(pp)$, for the Pomeron part alone. Instead, we can argue that this ratio should be less than 1, similar to $\sigma_{\text{tot}}^{(\mathbb{P})}(K^+p)/\sigma_{\text{tot}}^{(\mathbb{P})}(\pi^+p) < 1$; see Sec. 3.1 of Ref. [58]. The factor 0.9 in Eq. (4.1) is our educated guess. Data files and plots of various hadronic cross sections can be found in Ref. [59].

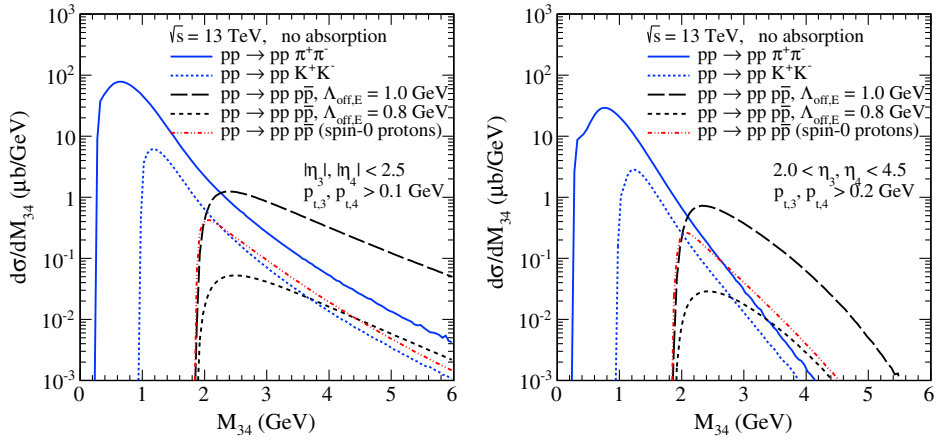

FIG. 2. The invariant-mass distributions for centrally produced $\pi^+\pi^-$, K^+K^-, and $p\bar{p}$ systems for different experimental conditions at $\sqrt{s} = 13$ TeV. Results for the combined tensor-Pomeron and Reggeon exchanges and $\Lambda_{\mathrm{off},E} = 1$ GeV are presented. For the $p\bar{p}$ production, we show results also for $\Lambda_{\mathrm{off},E} = 0.8$ GeV; see Eq. (2.14). No absorption effects were included here.

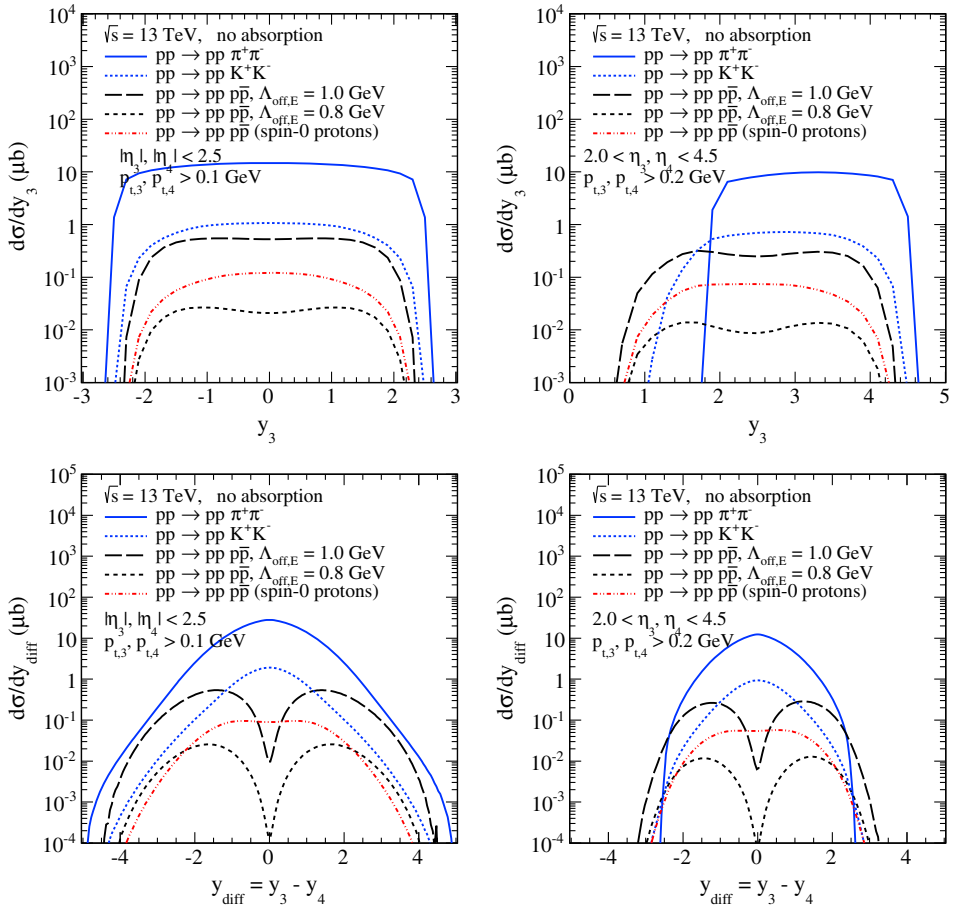

FIG. 3. The differential cross sections for various processes at $\sqrt{s} = 13$ TeV. In the top panels, we show the rapidity distributions obtained for the tensor Pomeron and Reggeon exchanges. In the bottom panels, we show the distributions in the rapidity difference between the centrally produced hadrons. No absorption effects were included here.

tensor-Pomeron approach was recently studied in Ref. [60]. For reference, we show also a naive ("spin-0 protons") result for artificially modified spin of centrally produced nucleons, from $1/2$ to 0; see the red dash-dotted line. Here, we assume the amplitude as for K^+K^- production but with some modifications, e.g., in the case of the $(\mathbb{P},\mathbb{P})$ term replacing m_K, $2\beta_{\mathbb{P}KK}$, and $F_M(t_{1,2})$ by m_p, $3\beta_{\mathbb{P}NN}$, and $F_1(t_{1,2})$, respectively. We take into account also Reggeon

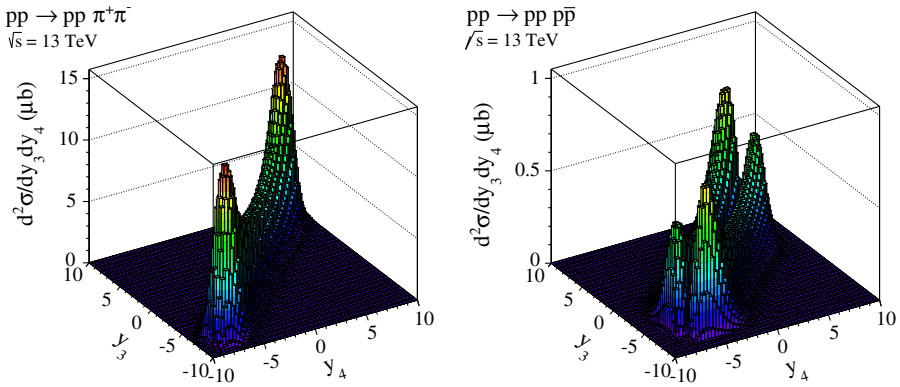

FIG. 4. The two-dimensional distributions in (y_3, y_4) for two processes at $\sqrt{s} = 13$ TeV. Results for the combined tensor-Pomeron and Reggeon exchanges are presented. We have taken here $\Lambda_{\text{off},E} = 1$ GeV; see Eq. (2.14). No absorption effects were included here. The asymmetry in the right panel will be discussed below.

exchanges with the corresponding Reggeon-nucleon-nucleon coupling parameters. This result is purely academic but illustrates how important the correct inclusion of the spin degrees of freedom is in the Regge calculation. Different spin of the produced particles clearly leads to different results.

In Fig. 2, we compare the invariant-mass distributions for the $\pi^+\pi^-$, K^+K^-, and $p\bar{p}$ cases for two different experimental conditions at $\sqrt{s} = 13$ TeV. In our calculations, we have included both Pomeron and Reggeon exchanges. The distribution in $p\bar{p}$ invariant mass has much larger threshold but is also much less steep, compared to that for production of pseudoscalar meson pairs. This effect is related to the spin of the produced particles (1/2 versus 0). We hope for a confirmation of the slope of the invariant-mass distribution, e.g., by the ATLAS or the ALICE collaboration. We see from Fig. 2 that the normalizations of the M_{34} distributions for $p\bar{p}$ are very sensitive to the cutoff parameter $\Lambda_{\text{off},E}$ of Eq. (2.14). In addition, we have the effects of absorption corrections. To fix the magnitudes of these two effects, we will have, at the moment, to have recourse to experimental input, which, presumably, will come soon.

In Fig. 3, we show the rapidity distributions (the top panels) and the distributions in rapidity difference $y_{\text{diff}} = y_3 - y_4$ (the bottom panels) for the ATLAS and LHCb pseudorapidity ranges. The distribution in the (anti)proton rapidity looks rather standard, while the distribution for y_{diff} is very special. We predict a dip in the rapidity difference between the antiproton and proton for $y_{\text{diff}} = 0$. The dip is caused by a good separation of $\hat{t}$ and $\hat{u}$ contributions in (y_3, y_4) space. This novel effect is inherently related to the spin 1/2 of the produced hadrons. We have checked that for the $p\bar{p}$ production the $\hat{t}$- and $\hat{u}$-channel diagrams interfere destructively for $(C_1, C_2) = (1, 1)$ and $(-1, -1)$ exchanges and constructively for $(1, -1)$ and $(-1, 1)$ exchanges. For the $\pi^+\pi^-$ production, we get the opposite interference effects between the $\hat{t}$- and $\hat{u}$-channel diagrams.

In Fig. 4, we show the two-dimensional distributions in rapidity of the π^+ and π^- (the left panel) and of the antiproton and proton (the right panel) for the full phase space. In our calculations, we have included both Pomeron and Reggeon exchanges. The Reggeon exchange contributions lead to enhancements of the cross section mostly at large rapidities of the centrally produced hadrons. For the production of the dipion continuum, the cross section is concentrated along the diagonal $y_3 = y_4$. For the production of $p\bar{p}$ pairs, one can observe that the dip extends over the whole diagonal in (y_3, y_4) space.

Figure 5 shows the asymmetry

$$A_{p\bar{p}}(\eta) = \frac{\frac{d\sigma}{d\eta_3}(\eta) - \frac{d\sigma}{d\eta_4}(\eta)}{\frac{d\sigma}{d\eta_3}(\eta) + \frac{d\sigma}{d\eta_4}(\eta)}, \tag{4.2}$$

where η_3 and η_4 are the pseudorapidities of the antiproton and proton, respectively, as a function of the pseudorapidity η at $\sqrt{s} = 13$ TeV. No absorption effects are included here, but they should approximately cancel in the ratio. Sizeable asymmetries are predicted in the full phase space. Much smaller asymmetries are seen for the limited range of pseudorapidities corresponding to the ATLAS, CMS, and ALICE experiments. The effect is better seen for the LHCb experiment, which covers the higher pseudorapidity region relevant for the Reggeon exchanges. The asymmetry is caused by the interference of the $(C_1, C_2) = (1, 1)$ and $(-1, -1)$ exchanges with the $(C_1, C_2) = (1, -1)$ and $(-1, 1)$ exchanges; see Eqs. (2.5)–(2.8). The former exchanges give an amplitude that is antisymmetric under $p_3 \leftrightarrow p_4$, whereas the latter exchanges give a symmetric amplitude under $p_3 \leftrightarrow p_4$; see Eq. (2.12) and the discussion following it. Thus, the resulting $p\bar{p}$ distribution will not be symmetric under $p_3 \leftrightarrow p_4$. The biggest contributions to the asymmetry come from the interference of the $(\mathbb{P}, \mathbb{P})$ term with the $(\mathbb{P}, \omega_{\mathbb{R}})$ and $(\omega_{\mathbb{R}}, \mathbb{P})$ contributions to the total amplitude. The prediction is that at larger $|\eta|$ more $\bar{p}$ than p should be observed, while at smaller $|\eta|$, the situation is reversed.

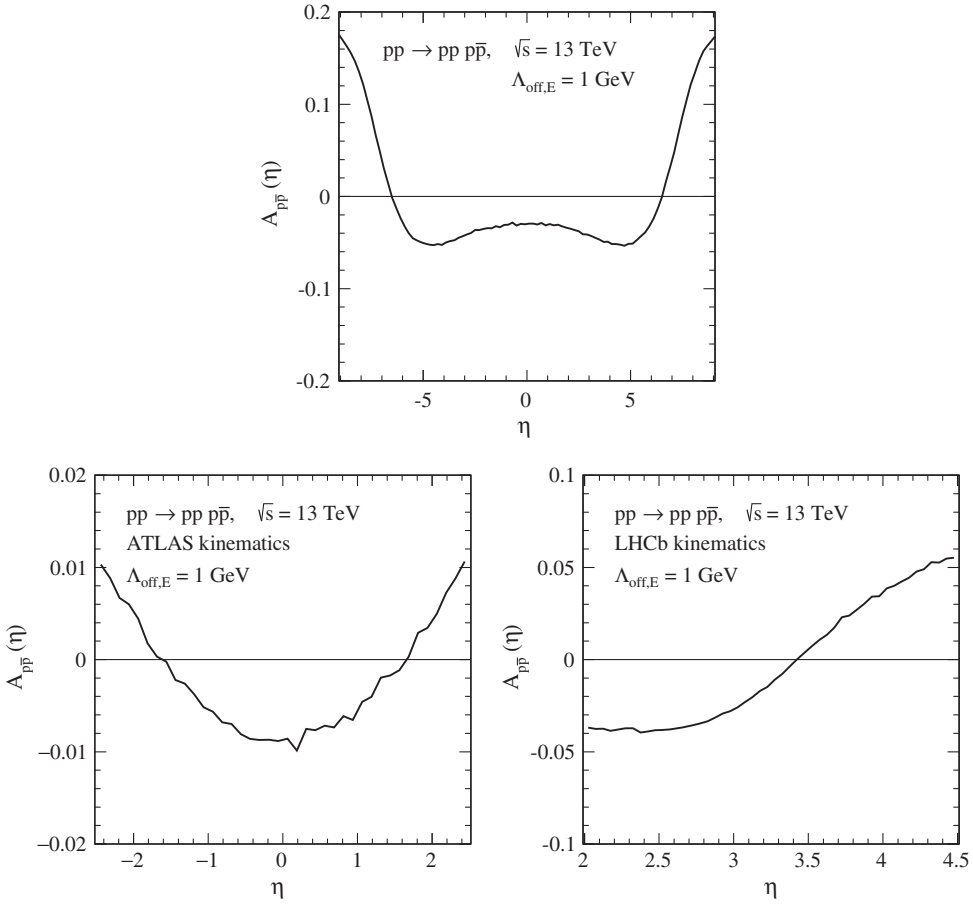

FIG. 5. The asymmetry $A_{p\bar{p}}(\eta)$ (4.2) as function of the pseudorapidity η for the full phase space (the top panel) and for the ATLAS and LHCb pseudorapidity ranges (the bottom panels) at $\sqrt{s} = 13$ TeV. Cuts on the transverse momenta of the centrally produced nucleons $p_{t,3}, p_{t,4} > 0.1$ and 0.2 GeV for the ATLAS and LHCb, respectively, have been imposed.

More general asymmetries than (4.2) can be considered and are again due to the interference of the $(C_1, C_2) = (1, 1)$ and $(-1, -1)$ with the $(C_1, C_2) = (1, -1)$ and $(-1, 1)$ exchanges. We emphasize that the following discussion holds for both nonresonant and resonant $p\bar{p}$ production. We can, for instance, consider the one-particle distributions for the central p and $\bar{p}$ in the overall c.m. system,

$$\frac{d^3\sigma}{d^3p_3}(\vec{p}_3) \quad \text{for the antiproton,}$$
$$\frac{d^3\sigma}{d^3p_4}(\vec{p}_4) \quad \text{for the proton,}$$

and the asymmetry

$$A^{(1)}(\vec{p}) = \frac{\frac{d^3\sigma}{d^3p_3}(\vec{p}) - \frac{d^3\sigma}{d^3p_4}(\vec{p})}{\frac{d^3\sigma}{d^3p_3}(\vec{p}) + \frac{d^3\sigma}{d^3p_4}(\vec{p})}. \tag{4.3}$$

Here, the leading protons $p(\vec{p}_1)$ and $p(\vec{p}_2)$ may be integrated over their whole or only a part of their phase space. We can also consider the two-particle cross section for the centrally produced p and $\bar{p}$: $\frac{d^6\sigma}{d^3p_3 d^3p_4}(\vec{p}_3, \vec{p}_4)$. A suitable asymmetry there is

$$A^{(2)}(\vec{p}, \vec{p}') = \frac{\frac{d^6\sigma}{d^3p_3 d^3p_4}(\vec{p}, \vec{p}') - \frac{d^6\sigma}{d^3p_3 d^3p_4}(\vec{p}', \vec{p})}{\frac{d^6\sigma}{d^3p_3 d^3p_4}(\vec{p}, \vec{p}') + \frac{d^6\sigma}{d^3p_3 d^3p_4}(\vec{p}', \vec{p})}. \tag{4.4}$$

In words, this asymmetry means the following. We choose two momenta $\vec{p}$ and $\vec{p}'$. Then, we ask if the situations $[\bar{p}(\vec{p}), p(\vec{p}')]$ and $[\bar{p}(\vec{p}'), p(\vec{p})]$ occur at the same or at a different rate.

Another asymmetry of this type can be constructed from the pseudorapidity distributions $\frac{d^2\sigma}{d\eta_3 d\eta_4}(\eta_3, \eta_4)$. For two pseudorapidities η and η', we define

$$\tilde{A}^{(2)}(\eta, \eta') = \frac{\frac{d^2\sigma}{d\eta_3 d\eta_4}(\eta, \eta') - \frac{d^2\sigma}{d\eta_3 d\eta_4}(\eta', \eta)}{\frac{d^2\sigma}{d\eta_3 d\eta_4}(\eta, \eta') + \frac{d^2\sigma}{d\eta_3 d\eta_4}(\eta', \eta)}. \tag{4.5}$$

For the quantity $\frac{d^2\sigma}{d\eta_3 d\eta_4}(\eta_3, \eta_4)$ and the asymmetry $\tilde{A}^{(2)}(\eta, \eta')$, we have also investigated effects of an Odderon using the parameters of Eqs. (A12)–(A14). In Fig. 6, we show, in two-dimensional plots, the ratios

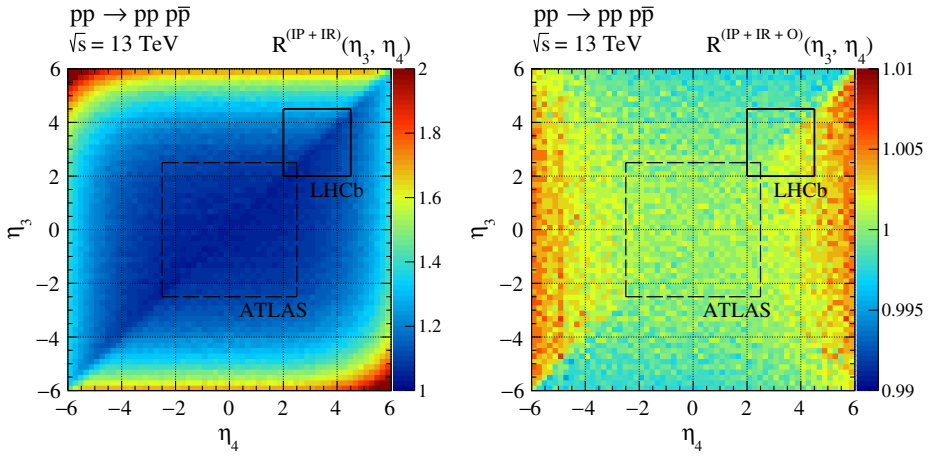

FIG. 6. The ratios $R(\eta_3,\eta_4)$ at $\sqrt{s}=13$ TeV and $p_{t,3}, p_{t,4} > 0.2$ GeV. The left panel represents the result for the ratio $R^{(\mathbb{P}+\mathbb{R})}(\eta_3,\eta_4)$ (4.6). The right panel shows the result for $R^{(\mathbb{P}+\mathbb{R}+\mathbb{O})}(\eta_3,\eta_4)$ (4.7). Note that different z scales are taken for the left and right panels. Calculations were done with the parameters of Appendix. In addition, regions of the coverage for the ATLAS and LHCb experiments are shown.

$$R^{(\mathbb{P}+\mathbb{R})}(\eta_3,\eta_4)=\frac{d^2\sigma^{(\mathbb{P}+\mathbb{R})}/d\eta_3 d\eta_4}{d^2\sigma^{(\mathbb{P})}/d\eta_3 d\eta_4}, \tag{4.6}$$

$$R^{(\mathbb{P}+\mathbb{R}+\mathbb{O})}(\eta_3,\eta_4)=\frac{d^2\sigma^{(\mathbb{P}+\mathbb{R}+\mathbb{O})}/d\eta_3 d\eta_4}{d^2\sigma^{(\mathbb{P}+\mathbb{R})}/d\eta_3 d\eta_4} \tag{4.7}$$

for $\sqrt{s}=13$ TeV and $-6\le\eta_3,\eta_4\le 6$. We see that in the limited range of pseudorapidities corresponding to the ATLAS and LHCb experiments the effects of the secondary Reggeons are predicted to be in the ranges of 2%–11% and 5%–26%, respectively. The addition of an Odderon with the parameters of Eq. (A14) has only an effect of less than 0.5%.

In Fig. 7, we show the asymmetry (4.5) including Pomeron and Reggeon exchanges. For the investigated pseudorapidity range, the asymmetries due to Pomeron plus Reggeon exchange show a characteristic pattern: positive for $|\eta|>|\eta'|$ and negative for $|\eta|<|\eta'|$. That is, antiprotons are predicted to come out typically with a higher absolute value of the (pseudo)rapidity than protons. In Fig. 7, the inclusion of the Odderon would hardly change the result, only at the level of less than 1%. This is less than theoretical uncertainties associated with the Reggeon exchanges.

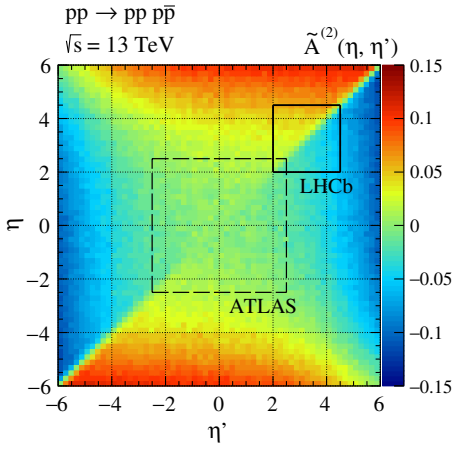

FIG. 7. The asymmetry $\tilde{A}^{(2)}(\eta,\eta')$ (4.5) at $\sqrt{s}=13$ TeV and $p_{t,3}, p_{t,4} > 0.2$ GeV. Shown is the result including Pomeron and Reggeon exchanges.

Finally, we note that for calculations of the asymmetries (4.2)–(4.5) it is essential to use a model in which the Pomeron is correctly treated as a $C=+1$ exchange, as is the case for our tensor Pomeron. On the other hand, in a vector-Pomeron model, using standard quantum field theory rules for the vertices, we will have effectively a $C=-1$ Pomeron. Then, all exchanges will be, effectively, $(C_1,C_2)=(-1,-1)$, and all asymmetries (4.2) to (4.5) will be zero. We cannot and do not exclude the possibility that by introducing some *ad hoc* sign changes in amplitudes one can generate nonzero asymmetries also in vector-Pomeron models. But we emphasize that in the tensor-Pomeron model [27] asymmetries are generated in a natural and straightforward way. Thus, experimental observations of such asymmetries would give strong support for the tensor-Pomeron concept.

Now, we turn to $p\bar{p}$ production via resonances. Not much is known about mesonic resonances in the $p\bar{p}$ channel, especially for those produced in the diffractive processes. Exceptions may be production of η_c and χ_c mesons for which the branching fractions to the $p\bar{p}$ channel are relatively well known [53]. There is also some evidence for the presence of the $f_2(1950)$ resonance in the $\gamma\gamma\to p\bar{p}$ reaction [39]. Although statistics of the ISR data [2,4] was poor for the $pp\to ppp\bar{p}$ reaction, the data show a large low-mass enhancement. With good statistics one could study at the LHC the distribution $d^2\sigma/dM_{34}dy_{\rm diff}$ for the $pp\to ppp\bar{p}$ reaction. In the right panel of Fig. 8, we show this distribution for the nonresonant $p\bar{p}$ production. For comparison, in the left panel of Fig. 8, the distribution for

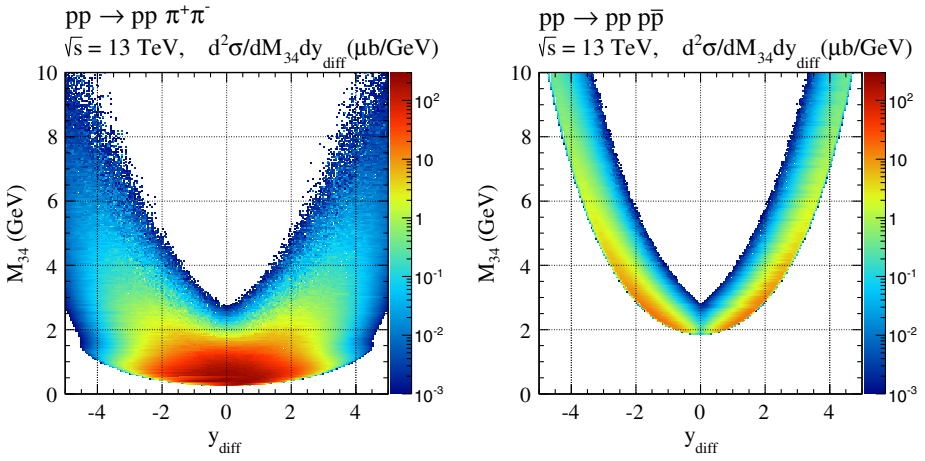

FIG. 8. The two-dimensional distributions in $(M_{34}, \mathrm{y_{diff}})$ for the diffractive continuum $\pi^+\pi^-$ (the left panel) and $p\bar{p}$ (the right panel) production for the full phase space at $\sqrt{s} = 13$ TeV. Results for the combined tensor-Pomeron and Reggeon exchanges are shown. We have taken here $\Lambda_{\mathrm{off},E} = 1$ GeV. No absorption effects have been included here.

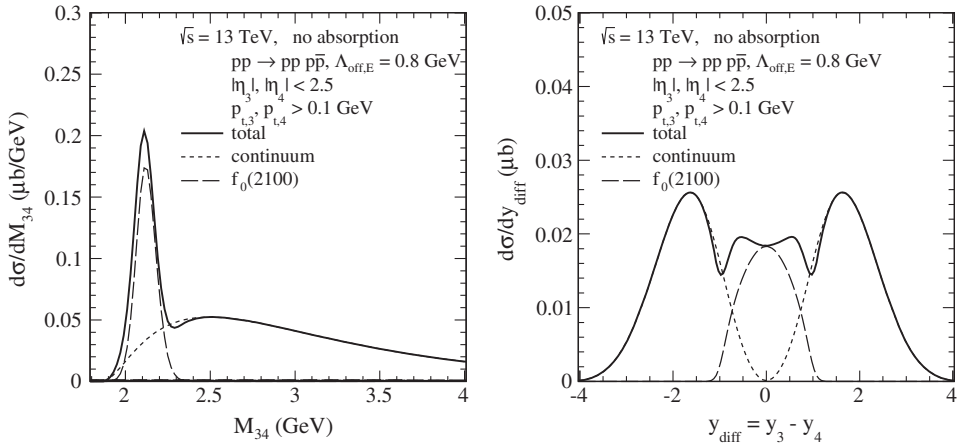

FIG. 9. The differential cross sections for $pp \to ppp\bar{p}$ at $\sqrt{s} = 13$ TeV for continuum plus $f_0(2100)$ production. The distributions in the $p\bar{p}$ invariant mass (the left panel) and in $\mathrm{y_{diff}}$ (the right panel) are shown. No absorption effects were included here.

the $pp \to pp\pi^+\pi^-$ reaction is shown. For $p\bar{p}$ production, one can observe a characteristic ridge at the edge of the $(M_{34}, \mathrm{y_{diff}})$ space. The interior is then free of the diffractive continuum. There, the identification of possible resonances should be easier. In reality, the presence of resonances may destroy the dip as resonances are expected to give a dominant contribution just at $\mathrm{y_{diff}} = 0$.

In Fig. 9, we discuss one possible scenario for the $pp \to ppp\bar{p}$ reaction. We take into account the nonresonant continuum including both Pomeron and Reggeon exchanges and, as an example, the scalar $f_0(2100)$ resonance created by the Pomeron-Pomeron fusion. The scalar $f_0(2100)$ was observed in $p\bar{p}$ annihilation into the $\eta\eta$ channel using a partial wave analysis of Crystal Barrel data [61,62]. It may be considered as a second scalar glueball, probably mixed with $q\bar{q}$ states. For the continuum term, we take $\Lambda_{\mathrm{off},E} = 0.8$ GeV in Eq. (2.14), while for the resonant term, we take $\Lambda_{f_0} = 1$ GeV in Eq. (3.4) and $g'_{\mathbb{P}\mathbb{P}f_0} g_{f_0 p\bar{p}} = 0.8$, $g''_{\mathbb{P}\mathbb{P}f_0} = 0$; see Eq. (3.2) and Appendix of Ref. [33]. Here, the coupling constants are fixed arbitrarily. We only want to give an example for the effects to be expected from resonance contributions. We show the distributions in the $p\bar{p}$ invariant mass (the left panel) and in $\mathrm{y_{diff}}$ (the right panel) at $\sqrt{s} = 13$ TeV. Clearly, the resonant contribution leads to enhancements at low $M_{p\bar{p}}$ and in the central region of $\mathrm{y_{diff}}$. We can see that the complete result indicates an interference effect of the continuum and $f_0(2100)$ terms. With the parameters used here, we get for the complete cross section 113 nb for the ATLAS cuts $(|\eta_3|, |\eta_4| < 2.5, p_{t,3}, p_{t,4} > 0.1$ GeV) and 35 nb for the LHCb cuts $(2 < \eta_3, \eta_4 < 4.5, p_{t,3}, p_{t,4} > 0.2$ GeV) on centrally produced $p\bar{p}$. Here, the absorption effects are not included. It is worth adding that the cross section for the resonant contribution is concentrated along the diagonal $\mathrm{y_3} \simeq \mathrm{y_4}$ in $(\mathrm{y_3}, \mathrm{y_4})$ space, exactly in the valley of the continuum contribution (see the right panel in Fig. 4).

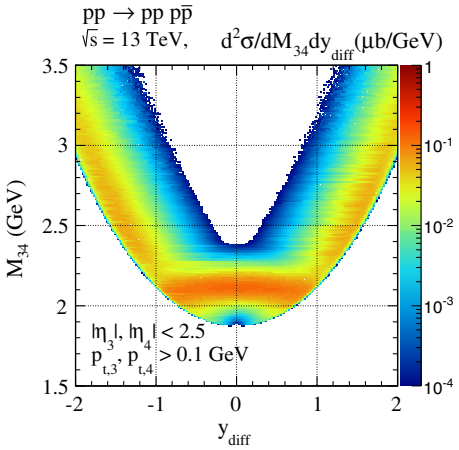

FIG. 10. The two-dimensional distribution in (M_{34}, y_{diff}) for the $p\bar{p}$ production at $\sqrt{s} = 13$ TeV including the continuum and the $f_0(2100)$ contribution. The strength of the resonance contribution is chosen arbitrarily. No absorption effects were included here.

In Fig. 10, we show two-dimensional distribution in (M_{34}, y_{diff}) for $pp \to ppp\bar{p}$ obtained from the nonresonant plus the $f_0(2100)$ resonant contributions. Here, the model parameters were chosen as in Fig. 9. Comparing with the right panel of Fig. 8, we see clearly that the resonance contribution is centered around $M_{34} = 2.1$ GeV and is approximately uniform in y_{diff} for $|y_{diff}| \lesssim 1$. Note that for $M_{34} \to 2m_p$, that is, for $\vec{p}_3 - \vec{p}_4 \to 0$ both, the dominant $(\mathbb{P}, \mathbb{P})$ continuum contribution as well as the $f_0(2100)$ resonance contribution must vanish; see Eq. (2.12). This is clearly seen in Fig. 10.

Also, azimuthal correlations are interesting for central exclusive $p\bar{p}$ production. From the experimental point of view, this typically would require that the momenta of the leading protons are measured. Then, one could study, for instance, the distributions in the angle ϕ_{12} between the transverse momenta $\vec{p}_{t,1}$ and $\vec{p}_{t,2}$ of the leading protons. For low-energy central-meson production, these angular distributions have been extensively discussed in Refs. [7–13], Refs. [63–65], and from the tensor-Pomeron point of view in Ref. [33]. Angular distributions for glueball production have been discussed in Ref. [32]. Since we have constructed in the present paper a model for central $p\bar{p}$ production at the amplitude level, we could also discuss such azimuthal correlations. We have checked that our model, including both the continuum and the scalar resonance $f_0(2100)$, taking into account only the $(l, S) = (0, 0)$ coupling in (3.2) gives a rather flat ϕ_{12} distribution, unlike for central $\pi^+\pi^-$ production [34,36]. This is consistent with a measurement made by the WA102 Collaboration; see Fig. 4(a) of Ref. [10]. But since present LHC experiments are not yet equipped for such measurements, we leave this for a further publication.

V. CONCLUSIONS

In the present article, we have discussed exclusive production of $p\bar{p}$ and $\Lambda\bar{\Lambda}$ pairs in proton-proton collisions. At the present stage, we have taken into account mainly the diffractive production of the $p\bar{p}$ continuum. The amplitudes have been calculated using Feynman rules within the tensor-Pomeron model [27] and taking into account the spins of the produced particles. Applying this model to our reactions here, we had to introduce some form factors containing suitable cutoff parameters; see Eqs. (2.14) and (3.4). A first estimate of these cutoff parameters was made by comparing to low-statistics ISR data in which mostly the integrated cross section for $pp \to ppp\bar{p}$ was measured at $\sqrt{s} = 62$ GeV. There, we need a cutoff parameter $\Lambda_{off,E} \sim 1$ GeV in Eq. (2.14). The form factors and corresponding cutoff parameters needed to describe the off-shellness of the intermediate t-/u-channel protons are not well known and have to be fitted in the future to experimental data. They influence mostly the absolute normalization of the cross sections and have almost no influence on shapes of distributions. In this paper, we did not concentrate on the absolute normalization but rather on relative effects by studying the qualitative features of the $pp \to ppp\bar{p}$ reaction in the tensor-Pomeron model. To describe the relatively low-energy ISR and WA102 experiments, we find that we have to include also subleading Reggeon exchanges in addition to the two-Pomeron exchange.

For our predictions for the LHC, we have used the off-shell proton form factor parameter in Eq. (2.14), $\Lambda_{off,E}$, in the range between 0.8 and 1 GeV. The invariant-mass distribution for $p\bar{p}$ pairs is predicted to extend to larger dihadron invariant masses than for the production of $\pi^+\pi^-$ or K^+K^- or artificial pseudoscalar nucleons. This is strongly related to spin 1/2 for nucleons versus spin 0 for pseudoscalar mesons.

Especially interesting is the distribution in the rapidity difference between antiproton and proton. For continuum $p\bar{p}$ production, we predict a dip at $y_{diff} = 0$, in contrast to $\pi^+\pi^-$ and K^+K^- production in which a maximum of the cross section occurs at $y_{diff} = 0$. The dip is caused by a good separation of $\hat{t}$ and $\hat{u}$ contributions in (y_3, y_4) space and destructive interference of them along the diagonal $y_3 = y_4$ characteristic for our Feynman diagrammatic calculation with correct treatment of spins.

In our calculations, we have included both Pomeron and Reggeon exchanges. The Reggeon exchange contributions lead to enhancements at large absolute values of the p and $\bar{p}$ (pseudo)rapidities. A similar effect was predicted for the $pp \to pp\pi^+\pi^-$ reaction in Ref. [22]. We have predicted asymmetries in the (pseudo)rapidity distributions of the centrally produced antiproton and proton. The asymmetry is caused by interference effects of the dominant $(\mathbb{P}, \mathbb{P})$ with the subdominant $(\mathbb{R}_-, \mathbb{P} + \mathbb{R}_+)$ and $(\mathbb{P} + \mathbb{R}_+, \mathbb{R}_-)$ exchanges. It should be emphasized that limited detector acceptances in experimental searches at the LHC might affect the size of the asymmetry. The asymmetry should be much more visible for the LHCb experiment, which covers a region of larger pseudorapidities where the Reggeon

exchanges become more relevant. Also, the Odderon will contribute to such asymmetries. However, we find for typical Odderon parameters allowed by recent pp elastic data [44] only very small effects, roughly a factor 10 smaller than the effects due to Reggeons as predicted in the present paper.

All our predictions here have been done for the tensor-Pomeron model. In the literature, often, a vector Pomeron is used, which is—strictly speaking—inconsistent with the rules of quantum field theory as it gives the Pomeron charge conjugation $C=-1$ instead of $C=+1$. This is discussed, e.g., in Refs. [27,28,36]. Although the vector-Pomeron model is incorrect from the field theory point of view, it leads to almost the same distributions including the prediction of the dip at $y_{\mathrm{diff}}=0$. This is not too surprising since the leading $(\mathbb{P},\mathbb{P})$ fusion term has $(C_1,C_2)=(1,1)$ for the tensor Pomeron and $(C_1,C_2)=(-1,-1)$ for the vector Pomeron, giving in both cases a state with $C=+1$. The situation is quite different for Pomeron-Reggeon, $(\mathbb{P},\mathbb{R}_-)$ and $(\mathbb{R}_-,\mathbb{P})$, exchange. There, we get with a tensor Pomeron a $C=-1$ state, with a vector Pomeron again a $C=+1$ state. The interference of $p\bar{p}$ amplitudes with $C=+1$ and $C=-1$ leads to the asymmetries discussed in Sec. IV. We see great difficulties producing such asymmetries in a vector-Pomeron model in which only $C=+1$ $p\bar{p}$ amplitudes occur. Therefore, we find it an important task for experimentalist to study the asymmetries (4.2)–(4.5). If nonzero asymmetries are found, we would have a further strong argument in favor of the tensor-Pomeron concept.

In the present study, we have focused mainly on the production of continuum $p\bar{p}$ pairs in the framework of the tensor-Pomeron model, treating correctly the spin degrees of freedom. Not much is known about diffractively produced $p\bar{p}$ resonances. Any experimentally observed distortions from our continuum-$p\bar{p}$ predictions may therefore signal the presence of resonances. This could give new interesting information for meson spectroscopy. We have discussed a first qualitative attempt to "reproduce" the experimentally observed behaviors of the $p\bar{p}$ invariant-mass (M_{34}) spectra observed in Refs. [2,4,10]. Our calculation shows that the diffractive production of $p\bar{p}$ through the s-channel $f_0(2100)$ resonance leads to an enhancement at low M_{34} and that the resonance contribution is concentrated at $|y_{\mathrm{diff}}|<1$. In general, more resonances can contribute, e.g., $f_0(2020)$, $f_0(2200)$, and $f_0(2300)$. Contributions of other states, such as $f_2(1950)$, are not excluded. Also, the subthreshold $m_R<2m_p$ resonances that would effectively generate a continuum $p\bar{p}$ contribution should be taken into account; see Ref. [39]. Interference effects between the continuum and resonant mechanisms certainly will occur; see Fig. 9.

The predictions made for $p\bar{p}$ production can be easily repeated for diffractive $\Lambda\bar{\Lambda}$ pair production. Here, the uncertainties for the continuum contribution are slightly larger than for the $p\bar{p}$ production (higher off-shell effects and less-known interaction parameters). However, here, the resonance contributions are expected to be much smaller if present at all. Any clear observation of a resonance in the $\Lambda\bar{\Lambda}$ channel would, therefore, be a sensation, and the result would definitely go to the Particle Data Book. On the other hand, a lack of such resonances would allow a verification of the minimum at $y_{\mathrm{diff}}=0$, which we predict using the correct treatment of the spin degrees of freedom in the Regge-like calculations of central exclusive baryon-antibaryon production.

ACKNOWLEDGMENTS

The authors are grateful to Leszek Adamczyk, Carlo Ewerz, and Rainer Schicker for discussions. This work was partially supported by the Polish National Science Centre Grant No. 2014/15/B/ST2/02528 and by the Center for Innovation and Transfer of Natural Sciences and Engineering Knowledge in Rzeszów.

APPENDIX: EFFECTIVE PROPAGATORS AND VERTICES FOR POMERON, REGGEON, AND ODDERON EXCHANGE

Here, we collect the expressions for our effective exchanges and vertex functions as given in Sec. 3 of Ref. [27] in order to make our present paper self-contained. For extensive discussions motivating the following expressions, we refer to Ref. [27].

Our effective Pomeron propagator reads

$$i\Delta^{(\mathbb{P})}_{\mu\nu,\kappa\lambda}(s,t)=\frac{1}{4s}\left(g_{\mu\kappa}g_{\nu\lambda}+g_{\mu\lambda}g_{\nu\kappa}-\frac{1}{2}g_{\mu\nu}g_{\kappa\lambda}\right)(-is\alpha'_{\mathbb{P}})^{\alpha_{\mathbb{P}}(t)-1} \tag{A1}$$

and fulfills the following relations:

$$\Delta^{(\mathbb{P})}_{\mu\nu,\kappa\lambda}(s,t)=\Delta^{(\mathbb{P})}_{\nu\mu,\kappa\lambda}(s,t)=\Delta^{(\mathbb{P})}_{\mu\nu,\lambda\kappa}(s,t)=\Delta^{(\mathbb{P})}_{\kappa\lambda,\mu\nu}(s,t),$$
$$g^{\mu\nu}\Delta^{(\mathbb{P})}_{\mu\nu,\kappa\lambda}(s,t)=0,\qquad g^{\kappa\lambda}\Delta^{(\mathbb{P})}_{\mu\nu,\kappa\lambda}(s,t)=0. \tag{A2}$$

Here, the Pomeron trajectory $\alpha_{\mathbb{P}}(t)$ is assumed to be of standard linear form, see, e.g., Ref. [58],

$$\alpha_{\mathbb{P}}(t)=\alpha_{\mathbb{P}}(0)+\alpha'_{\mathbb{P}}t,$$
$$\alpha_{\mathbb{P}}(0)=1.0808,$$
$$\alpha'_{\mathbb{P}}=0.25\ \mathrm{GeV}^{-2}. \tag{A3}$$

The Pomeron-proton vertex function, supplemented by a vertex form factor, taken here to be the Dirac electromagnetic form factor of the proton for simplicity, has the form

$$
\begin{aligned}
&i\Gamma_{\mu\nu}^{(\mathbb{P}pp)}(p',p)\\
&= i\Gamma_{\mu\nu}^{(\mathbb{P}\bar{p}\,\bar{p})}(p',p)\\
&= -i3\beta_{\mathbb{P}NN}F_1((p'-p)^2)\\
&\quad\times\left\{\frac{1}{2}[\gamma_\mu(p'+p)_\nu+\gamma_\nu(p'+p)_\mu]-\frac{1}{4}g_{\mu\nu}(\not{p}'+\not{p})\right\},
\end{aligned}
\tag{A4}
$$

with $\beta_{\mathbb{P}NN}=1.87\ \text{GeV}^{-1}$.

The ansatz for the $C=+1$ Reggeons $\mathbb{R}_+=f_{2\mathbb{R}},a_{2\mathbb{R}}$ is similar to Eqs. (A1)–(A4). The $\mathbb{R}_+$ propagator is obtained from Eq. (A1) with the replacements

$$
\begin{aligned}
\alpha_{\mathbb{P}}(t)\to\alpha_{\mathbb{R}_+}(t)&=\alpha_{\mathbb{R}_+}(0)+\alpha'_{\mathbb{R}_+}t,\\
\alpha_{\mathbb{R}_+}(0)&=0.5475,\\
\alpha'_{\mathbb{R}_+}&=0.9\ \text{GeV}^{-2}.
\end{aligned}
\tag{A5}
$$

The $f_{2\mathbb{R}}$- and $a_{2\mathbb{R}}$-proton vertex functions are obtained from Eq. (A4) with the replacements ($M_0=1$ GeV)

$$
3\beta_{\mathbb{P}NN}\to\frac{g_{f_{2\mathbb{R}}pp}}{M_0},\qquad g_{f_{2\mathbb{R}}pp}=11.04
\tag{A6}
$$

and

$$
3\beta_{\mathbb{P}NN}\to\frac{g_{a_{2\mathbb{R}}pp}}{M_0},\qquad g_{a_{2\mathbb{R}}pp}=1.68,
\tag{A7}
$$

respectively.

Our ansatz for the $C=-1$ Reggeons $\mathbb{R}_-=\omega_{\mathbb{R}},\rho_{\mathbb{R}}$ reads as follows. We assume an effective vector propagator

$$
i\Delta_{\mu\nu}^{(\mathbb{R}_-)}(s,t)=ig_{\mu\nu}\frac{1}{M_-^2}(-is\alpha'_{\mathbb{R}_-})^{\alpha_{\mathbb{R}_-}(t)-1},
\tag{A8}
$$

with

$$
\begin{aligned}
&\alpha_{\mathbb{R}_-}(t)=\alpha_{\mathbb{R}_-}(0)+\alpha'_{\mathbb{R}_-}t,\qquad \alpha_{\mathbb{R}_-}(0)=0.5475,\\
&\alpha'_{\mathbb{R}_-}=0.9\ \text{GeV}^{-2},\qquad M_-=1.41\ \text{GeV}.
\end{aligned}
\tag{A9}
$$

The $\mathbb{R}_-$-proton vertex reads ($\mathbb{R}_-=\omega_{\mathbb{R}},\rho_{\mathbb{R}}$)

$$
\begin{aligned}
i\Gamma_{\mu}^{(\mathbb{R}_-pp)}(p',p)&=-i\Gamma_{\mu}^{(\mathbb{R}_-\bar{p}\,\bar{p})}(p',p)\\
&=-ig_{\mathbb{R}_-pp}F_1((p'-p)^2)\gamma_\mu,
\end{aligned}
\tag{A10}
$$

with

$$
\begin{aligned}
g_{\omega_{\mathbb{R}}pp}&=8.65,\\
g_{\rho_{\mathbb{R}}pp}&=2.02.
\end{aligned}
\tag{A11}
$$

Our ansatz for the Odderon follows Eqs. (3.16), (3.17) and (3.68), (3.69) of Ref. [27]:

$$
i\Delta_{\mu\nu}^{(\mathbb{O})}(s,t)=-ig_{\mu\nu}\frac{\eta_{\mathbb{O}}}{M_0^2}(-is\alpha'_{\mathbb{O}})^{\alpha_{\mathbb{O}}(t)-1},
\tag{A12}
$$

$$
\begin{aligned}
i\Gamma_{\mu}^{(\mathbb{O}pp)}(p',p)&=-i\Gamma_{\mu}^{(\mathbb{O}\bar{p}\,\bar{p})}(p',p)\\
&=-i3\beta_{\mathbb{O}pp}M_0F_1((p'-p)^2)\gamma_\mu.
\end{aligned}
\tag{A13}
$$

We take here what we think are representative values for the Odderon parameters in light of the recent TOTEM results [44],

$$
\begin{aligned}
\eta_{\mathbb{O}}&=-1,\\
\alpha_{\mathbb{O}}(t)&=\alpha_{\mathbb{O}}(0)+\alpha'_{\mathbb{O}}t,\\
\alpha_{\mathbb{O}}(0)&=1.05,\\
\alpha'_{\mathbb{O}}&=0.25\ \text{GeV}^{-2},\\
\beta_{\mathbb{O}NN}&=0.2\ \text{GeV}^{-1}.
\end{aligned}
\tag{A14}
$$

All numbers for the parameters listed above should be considered as default values to be checked and—if necessary—adjusted using relevant experimental data. Some estimates of the present uncertainties of the parameters are discussed in Sec. 3 of Ref. [27].

[1] R. Waldi, K. R. Schubert, and K. Winter, Search for glueballs in a pomeron pomeron scattering experiment, Z. Phys. C **18**, 301 (1983).

[2] T. Åkesson *et al.* (AFS Collaboration), A search for glueballs and a study of double pomeron exchange at the CERN Intersecting Storage Rings, Nucl. Phys. **B264**, 154 (1986).

[3] A. Breakstone *et al.* (ABCDHW Collaboration), Production of the f^0 meson in the Double Pomeron Exchange reaction $pp\to pp\pi^+\pi^-$ at $\sqrt{s}=62$ GeV, Z. Phys. C **31**, 185 (1986).

[4] A. Breakstone *et al.* (ABCDHW Collaboration), Inclusive Pomeron-Pomeron interactions at the CERN ISR, Z. Phys. C **42**, 387 (1989); Erratum **43**, 522(E) (1989).

[5] A. Breakstone *et al.* (ABCDHW Collaboration), The reaction Pomeron-Pomeron $\to\pi^+\pi^-$ and an unusual production mechanism for the $f_2(1270)$, Z. Phys. C **48**, 569 (1990).

[6] M. G. Albrow, T. D. Coughlin, and J. R. Forshaw, Central exclusive particle production at high energy hadron colliders, Prog. Part. Nucl. Phys. **65**, 149 (2010).

[7] D. Barberis *et al.* (WA102 Collaboration), A kinematical selection of glueball candidates in central production, Phys. Lett. B **397**, 339 (1997).

[8] D. Barberis *et al.* (WA102 Collaboration), A study of the centrally produced $\pi^+\pi^-\pi^+\pi^-$ channel in pp interactions at 450 GeV/c, Phys. Lett. B **413**, 217 (1997).

[9] D. Barberis *et al.* (WA102 Collaboration), A study of pseudoscalar states produced centrally in pp interactions at 450 GeV/c, Phys. Lett. B **427**, 398 (1998).

[10] D. Barberis *et al.* (WA102 Collaboration), A study of the centrally produced baryon—anti-baryon systems in pp interactions at 450 GeV/c, Phys. Lett. B **446**, 342 (1999).

[11] D. Barberis *et al.* (WA102 Collaboration), A coupled channel analysis of the centrally produced K^+K^- and $\pi^+\pi^-$ final states in pp interactions at 450 GeV/c, Phys. Lett. B **462**, 462 (1999).

[12] D. Barberis *et al.* (WA102 Collaboration), A study of the $f_0(1370)$, $f_0(1500)$, $f_0(2000)$ and $f_2(1950)$ observed in the centrally produced 4π final states, Phys. Lett. B **474**, 423 (2000).

[13] A. Kirk, Resonance production in central pp collisions at the CERN Omega Spectrometer, Phys. Lett. B **489**, 29 (2000).

[14] T. A. Aaltonen *et al.* (CDF Collaboration), Measurement of central exclusive $\pi^+\pi^-$ production in $p\bar{p}$ collisions at $\sqrt{s} = 0.9$ and 1.96 TeV at CDF, Phys. Rev. D **91**, 091101 (2015).

[15] V. Khachatryan *et al.* (CMS Collaboration), Exclusive and semi-exclusive $\pi^+\pi^-$ production in proton-proton collisions at $\sqrt{s} = 7$ TeV, Report Nos. CMS-FSQ-12-004; CERN-EP-2016-261.

[16] R. Staszewski, P. Lebiedowicz, M. Trzebiński, J. Chwastowski, and A. Szczurek, Exclusive $\pi^+\pi^-$ Production at the LHC with Forward Proton Tagging, Acta Phys. Pol. B **42**, 1861 (2011).

[17] L. Adamczyk, W. Guryn, and J. Turnau, Central exclusive production at RHIC, Int. J. Mod. Phys. A **29**, 1446010 (2014).

[18] R. Sikora (STAR Collaboration), Central exclusive production in the STAR experiment at RHIC, AIP Conf. Proc. **1819**, 040012 (2017).

[19] J. Pumplin and F. S. Henyey, Double pomeron exchange in the reaction $pp \to pp\pi^+\pi^-$, Nucl. Phys. **B117**, 377 (1976).

[20] P. Lebiedowicz and A. Szczurek, Exclusive $pp \to pp\pi^+\pi^-$ reaction: From the threshold to LHC, Phys. Rev. D **81**, 036003 (2010).

[21] P. Lebiedowicz, R. Pasechnik, and A. Szczurek, Measurement of exclusive production of scalar χ_{c0} meson in proton-(anti)proton collisions via $\chi_{c0} \to \pi^+\pi^-$ decay, Phys. Lett. B **701**, 434 (2011).

[22] P. Lebiedowicz and A. Szczurek, Exclusive $pp \to nn\pi^+\pi^+$ reaction at LHC and RHIC, Phys. Rev. D **83**, 076002 (2011).

[23] P. Lebiedowicz and A. Szczurek, $pp \to ppK^+K^-$ reaction at high energies, Phys. Rev. D **85**, 014026 (2012).

[24] R. Kycia, P. Lebiedowicz, A. Szczurek, and J. Turnau, Triple Regge exchange mechanisms of four-pion continuum production in the $pp \to pp\pi^+\pi^-\pi^+\pi^-$ reaction, Phys. Rev. D **95**, 094020 (2017).

[25] L. A. Harland-Lang, V. A. Khoze, and M. G. Ryskin, Modelling exclusive meson pair production at hadron colliders, Eur. Phys. J. C **74**, 2848 (2014).

[26] P. Lebiedowicz and A. Szczurek, Revised model of absorption corrections for the $pp \to pp\pi^+\pi^-$ process, Phys. Rev. D **92**, 054001 (2015).

[27] C. Ewerz, M. Maniatis, and O. Nachtmann, A model for soft high-energy scattering: Tensor Pomeron and vector odderon, Ann. Phys. (Amsterdam) **342**, 31 (2014).

[28] C. Ewerz, P. Lebiedowicz, O. Nachtmann, and A. Szczurek, Helicity in proton-proton elastic scattering and the spin structure of the Pomeron, Phys. Lett. B **763**, 382 (2016).

[29] L. Adamczyk *et al.* (STAR Collaboration), Single spin asymmetry A_N in polarized proton-proton elastic scattering at $\sqrt{s} = 200$ GeV, Phys. Lett. B **719**, 62 (2013).

[30] O. Nachtmann, Considerations concerning diffraction scattering in quantum chromodynamics, Ann. Phys. (N.Y.) **209**, 436 (1991).

[31] S. K. Domokos, J. A. Harvey, and N. Mann, Pomeron contribution to pp and $p\bar{p}$ scattering in AdS/QCD, Phys. Rev. D **80**, 126015 (2009).

[32] I. Iatrakis, A. Ramamurti, and E. Shuryak, Pomeron interactions from the Einstein-Hilbert Action, Phys. Rev. D **94**, 045005 (2016).

[33] P. Lebiedowicz, O. Nachtmann, and A. Szczurek, Exclusive central diffractive production of scalar and pseudoscalar mesons; tensorial vs. vectorial pomeron, Ann. Phys. (Amsterdam) **344**, 301 (2014).

[34] P. Lebiedowicz, O. Nachtmann, and A. Szczurek, ρ^0 and Drell-Söding contributions to central exclusive production of $\pi^+\pi^-$ pairs in proton-proton collisions at high energies, Phys. Rev. D **91**, 074023 (2015).

[35] A. Bolz, C. Ewerz, M. Maniatis, O. Nachtmann, M. Sauter, and A. Schöning, Photoproduction of $\pi^+\pi^-$ pairs in a model with tensor-pomeron and vector-odderon exchange, J. High Energy Phys. 01 (2015) 151.

[36] P. Lebiedowicz, O. Nachtmann, and A. Szczurek, Central exclusive diffractive production of the $\pi^+\pi^-$ continuum, scalar, and tensor resonances in pp and $p\bar{p}$ scattering within the tensor Pomeron approach, Phys. Rev. D **93**, 054015 (2016).

[37] P. Lebiedowicz, O. Nachtmann, and A. Szczurek, Exclusive diffractive production of $\pi^+\pi^-\pi^+\pi^-$ via the intermediate $\sigma\sigma$ and $\rho\rho$ states in proton-proton collisions within tensor Pomeron approach, Phys. Rev. D **94**, 034017 (2016).

[38] P. Lebiedowicz, O. Nachtmann, and A. Szczurek, Central production of ρ^0 in pp collisions with single proton diffractive dissociation at the LHC, Phys. Rev. D **95**, 034036 (2017).

[39] M. Kłusek-Gawenda, P. Lebiedowicz, O. Nachtmann, and A. Szczurek, From the $\gamma\gamma \to p\bar{p}$ reaction to the production of $p\bar{p}$ pairs in ultraperipheral ultrarelativistic heavy-ion collisions at the LHC, Phys. Rev. D **96**, 094029 (2017).

[40] C. C. Kuo *et al.* (Belle Collaboration), Measurement of $\gamma\gamma \to p\bar{p}$ production at Belle, Phys. Lett. B **621**, 41 (2005).

[41] L. Łukaszuk and B. Nicolescu, A possible interpretation of pp rising total cross-sections, Lett. Nuovo Cimento **8**, 405 (1973).

[42] D. Joynson, E. Leader, B. Nicolescu, and C. Lopez, Non-Regge and hyper-Regge effects in pion-nucleon charge

exchange scattering at high energies, Nuovo Cimento A **30**, 345 (1975).
[43] C. Ewerz, The odderon in quantum chromodynamics, arXiv:hep-ph/0306137.
[44] G. Antchev *et al.* (TOTEM Collaboration), First determination of the ρ parameter at $\sqrt{s} = 13$ TeV—Probing the existence of a colourless three-gluon bound state, Report No. CERN-EP-2017-335.
[45] E. Martynov and B. Nicolescu, Did TOTEM experiment discover the Odderon?, Phys. Lett. B **778**, 414 (2018).
[46] V. A. Khoze, A. D. Martin, and M. G. Ryskin, Elastic proton-proton scattering at 13 TeV, Phys. Rev. D **97**, 034019 (2018).
[47] V. A. Khoze, A. D. Martin, and M. G. Ryskin, Black disk, maximal Odderon and unitarity, Phys. Lett. B **780**, 352 (2018).
[48] F. E. Low, Model of the bare Pomeron, Phys. Rev. D **12**, 163 (1975).
[49] S. Nussinov, Colored-Quark Version of Some Hadronic Puzzles, Phys. Rev. Lett. **34**, 1286 (1975).
[50] E. A. Kuraev, L. N. Lipatov, and V. S. Fadin, The Pomeranchuk singularity in non-Abelian gauge theories, Zh. Eksp. Teor. Fiz. **72**, 377 (1977) [Sov. Phys. JETP **45**, 199 (1977)].
[51] I. I. Balitsky and L. N. Lipatov, The Pomeranchuk singularity in quantum chromodynamics, Yad. Fiz. **28**, 1597 (1978) [Sov. J. Nucl. Phys. **28**, 822 (1978)].
[52] R. A. Kycia, J. Chwastowski, R. Staszewski, and J. Turnau, GenEx: A simple generator structure for exclusive processes in high energy collisions, arXiv:1411.6035.
[53] C. Patrignani *et al.* (Particle Data Group Collaboration), Review of particle physics, Chin. Phys. C **40**, 100001 (2016).
[54] G. Alexander, U. Karshon, A. Shapira, G. Yekutieli, R. Engelmann, H. Filthuth, and W. Lughofer, Study of the $\Lambda - N$ system in low-energy $\Lambda - p$ elastic scattering, Phys. Rev. **173**, 1452 (1968).
[55] D. Bassano, C. Y. Chang, M. Goldberg, T. Kikuchi, and J. Leitner, Lambda-proton interactions at high energies, Phys. Rev. **160**, 1239 (1967).
[56] J. A. Kadyk, G. Alexander, J. H. Chan, P. Gaposchkin, and G. H. Trilling, Λp interactions in momentum range 300 to 1500 MeV/c, Nucl. Phys. **B27**, 13 (1971).
[57] S. Gjesdal, G. Presser, P. Steffen, J. Steinberger, F. Vannucci, H. Wahl, K. Kleinknecht, V. Lüth, and G. Zech, A measurement of the total cross-sections for Λ hyperon interactions on protons and neutrons in the momentum range from 6 GeV/c to 21 GeV/c, Phys. Lett. **B40**, 152 (1972).
[58] A. Donnachie, H. G. Dosch, P. V. Landshoff, and O. Nachtmann, Pomeron physics and QCD, Cambridge Monogr. Part. Phys., Nucl. Phys., Cosmol. **19**, 1 (2002).
[59] http://pdg.lbl.gov/2017/hadronic-xsections/hadron.html.
[60] P. Lebiedowicz, O. Nachtmann, and A. Szczurek, Towards a complete study of central exclusive production of the K^+K^- pairs in proton-proton collisions within the tensor pomeron approach, arXiv:1804.04706.
[61] A. V. Anisovich *et al.*, Partial wave analysis of $\bar{p}p \to \pi^-\pi^+$, $\pi^0\pi^0$, $\eta\eta$ and $\eta\eta'$, Nucl. Phys. **A662**, 319 (2000).
[62] A. V. Anisovich, C. A. Baker, C. J. Batty, D. V. Bugg, C. Hodd, J. Kisiel, V. A. Nikonov, A. V. Sarantsev, V. V. Sarantsev, and B. S. Zou, Data on $\bar{p}p \to \pi^0\pi^0$, $\eta\eta$ and $\eta\eta'$ from 600 to 1940 MeV/c, Nucl. Phys. **A662**, 344 (2000).
[63] F. E. Close and G. A. Schuler, Central production of mesons: Exotic states versus pomeron structure, Phys. Lett. B **458**, 127 (1999).
[64] F. E. Close and G. A. Schuler, Evidence that the pomeron transforms as a nonconserved vector current, Phys. Lett. B **464**, 279 (1999).
[65] F. E. Close, A. Kirk, and G. A. Schuler, Dynamics of glueball and $q\bar{q}$ production in the central region of pp collisions, Phys. Lett. B **477**, 13 (2000).